Nonlinear Stage of Modulational Instability in Repulsive Two-Component Bose-Einstein Condensates

S. Mossman,[1,2] S. I. Mistakidis,[3] G. C. Katsimiga,[3] A. Romero-Ros,[4,5] G. Biondini,[6] P. Schmelcher,[7,8] P. Engels,[2] and P. G. Kevrekidis[9]

[1]*Department of Physics and Biophysics, University of San Diego, San Diego, California 92110, USA*
[2]*Department of Physics and Astronomy, Washington State University, Pullman, Washington 99164-2814, USA*
[3]*Department of Physics and LAMOR, Missouri University of Science and Technology, Rolla, Missouri 65409, USA*
[4]*Departament de Física Quàntica i Astrofísica (FQA), Universitat de Barcelona (UB), Martí i Franqués, 1, 08028 Barcelona, Spain*
[5]*Institut de Ciències del Cosmos (ICCUB), Universitat de Barcelona (UB), Martí i Franqués, 1, 08028 Barcelona, Spain*
[6]*Department of Mathematics, State University of New York, Buffalo, New York 14260, USA*
[7]*Center for Optical Quantum Technologies, Department of Physics, University of Hamburg, Luruper Chaussee 149, 22761 Hamburg, Germany*
[8]*The Hamburg Centre for Ultrafast Imaging, University of Hamburg, Luruper Chaussee 149, 22761 Hamburg, Germany*
[9]*Department of Mathematics and Statistics, University of Massachusetts Amherst, Amherst, Massachusetts 01003-4515, USA*

(Received 21 February 2025; accepted 14 August 2025; published 10 September 2025)

Modulational instability (MI) is a fundamental phenomenon in the study of nonlinear dynamics, spanning diverse areas such as shallow water waves, optics, and ultracold atomic gases. In particular, the nonlinear stage of MI has recently been a topic of intense exploration and has been shown to manifest, in many cases, in the generation of dispersive shock waves (DSWs). In this Letter, we experimentally probe the MI dynamics in an immiscible two-component ultracold atomic gas with exclusively repulsive interactions, catalyzed by a hard-wall-like boundary produced by a repulsive optical barrier. We analytically describe the expansion rate of the DSWs in this system, generalized to arbitrary intercomponent interaction strengths and species ratios. We observe excellent agreement among the analytical results, an effective 1D numerical model, full 3D numerical simulations, and experimental data. Additionally, we extend this scenario to the interaction between two counterpropagating DSWs, which leads to the production of Peregrine soliton structures. These results further demonstrate the versatility of atomic platforms toward the controlled realization of DSWs and rogue waves.

DOI: 10.1103/6jsr-f8q1

Introduction—One of the most universal characteristics of nonlinear media, whether in water waves, acoustics, or nonlinear optics, is the susceptibility of plane waves to minor disturbances, known as modulational instability (MI) [1]. MI is a topic of active theoretical and experimental investigation, both in its own right [2] and as a tool to produce solitary waves across dimensions [3] and fields of application [4–7].

The linear stage of MI is characterized by an exponential growth of perturbations with small wave numbers, as verified by linearizing the governing equations around a uniform background. However, when such perturbations grow to a size comparable to the background, their dynamics enter a more complex regime referred to as the nonlinear stage of MI [8,9]. The simplest dynamical model for the description of MI is the single-component self-focusing nonlinear Schrödinger (NLS) equation in one dimension with cubic nonlinearity. It was conjectured, in Ref. [10], that the nonlinear stage of MI in the NLS equation is described by certain self-similar solutions of the corresponding Whitham modulation equations [11]. Such solutions were shown to arise from a large class of initial conditions [9] using the inverse scattering transform for the focusing NLS equation with nonzero background [12]. The nonlinear stage of MI was later observed in optical fiber experiments [13,14], water waves [15], and similar phenomena were, then, also shown to arise in more general NLS-type systems [16].

Ultracold atom quantum simulators provide highly controllable platforms that enable the realization of complex nonequilibrium phenomena, thanks to their exquisite tunability in terms of system parameters [17–19]. In this context, MI has been examined predominantly in the setting of single-component gases, as a means of generating bright soliton trains [20,21]. Real-time imaging has further elucidated these soliton features (growing sidebands, adjacent soliton phase, etc.) in more recent studies [22,23]. In higher dimensions, MI was also leveraged to induce fragmentation, producing Townes solitons in two dimensions [24,25] and self-patterned Townes-soliton necklaces in the presence of a vortex [26]. However, the nonlinear stage of MI has not yet been observed in repulsive (defocusing) multicomponent atomic systems. The latter setting has recently been exploited for a diverse palette of experiments to study effectively attractive dynamics, ranging from the formation of Townes solitons [27] in quasi-two-dimensional condensates [28] to that of rogue waves in the form of Peregrine solitons (PS) in effectively one-dimensional systems [29]. The interplay of the repulsive interactions and the resulting effective dynamics of the full system, as well as the richness of the multicomponent setting, render this a particularly useful and versatile platform.

In this Letter, we experimentally and theoretically demonstrate the emergence of MI in a defocusing multicomponent medium consisting of two hyperfine states of a ^{87}Rb Bose-Einstein condensate (BEC). Specifically, we analytically characterize the nonlinear stage of MI in this system by investigating the dynamical effects produced by the presence of a hard repulsive barrier enforcing a dam-break problem [30,31], namely, step-like initial conditions with zero velocity. Previous studies (starting with the theoretical analysis of Ref. [32]) have primarily focused on asymmetric settings [28,29,33,34] consisting of a majority and a minority component, leading to effective single-component self-focusing dynamics. In contrast, here, we showcase the manifestation of features such as MI and rogue waves for arbitrary particle ratios between the immiscible components, all the way to equal atom mixtures. This constitutes a fundamental feature of this work and a key digression from earlier studies, since MI dynamics indisputably emerges even though our purely repulsively interacting balanced mixtures allow no reduction to an effectively attractive system. Excellent agreement among experiment and three-dimensional (3D) mean-field theory is observed. This setup enables a quantitative characterization of the emergent nonstationary, coherent, nonlinear oscillatory structures referred to as dispersive shock waves (DSWs), previously experimentally realized in repulsive single-component BECs [35,36], and it also enables the potential realization of collisions between them. The latter are experimentally achieved by utilizing a geometry of two repulsive barriers, mimicking a matter-wave cavity which triggers the interference of multiple dam breaks and leads to the formation of a PS [29].

Experimental results—We begin with a BEC of approximately 9×10^5 ^{87}Rb atoms in an elongated optical trap with frequencies $\omega_{x,y,z} = 2\pi \times (2.5, 246, 261)$ Hz. The BEC is prepared in the $|F, m_F\rangle = |1, -1\rangle$ state in the presence of a narrow Gaussian beam generated by a 660 nm laser. The beam produces a repulsive barrier for the atoms that is placed at the center of the trap, with widths $s_x = 7.5$ and $s_y = 59.8$ μm and a potential height corresponding to approximately $I_0 = 300$ nK, sufficient to completely split the condensate. This initial state shows no meaningful dynamics over long timescales if left as a single spin component [37]. To initiate dynamics, we use fast microwave and rf pulses to prepare a mixture of the $|1, 0\rangle$ state with the $|2, 0\rangle$ state. This procedure results in a highly reproducible initial state, followed by MI features deterministically seeded by the edge of the stationary barrier. There is a slight atom loss with an exponential decay time of approximately 220 ms for the atoms in the $|2, 0\rangle$ state, which, however, we have fully taken into account in the numerical simulations and find that it does not significantly impact the dynamics.

A principal experimental result of this work is summarized in Figs. 1(a)–1(c). Figure 1(a) shows an example of a single experimental absorption image taken 60 ms after the preparation of an equally populated spin mixture, with the $|2, 0\rangle$ state appearing as the upper cloud and $|1, 0\rangle$ as the lower cloud in the panel. Each image is taken after 14 ms of free fall, allowing the $|2, 0\rangle$ state to be transferred back to the $|1, -1\rangle$ state, followed by a Stern-Gerlach process to image the two spin components simultaneously. Figure 1(b) depicts the integrated cross sections corresponding to Fig. 1(a) but averaged over 20 independent experimental realizations. The complementarity of the density modulations in the two spin states demonstrates the energy scale of these excitations—the instability excites spin oscillation modes without significantly affecting the overall condensate density. Moving forward, we present only the $|2, 0\rangle$ state recognizing that the $|1, 0\rangle$ state forms a complementary pattern.

The experimental procedure is repeated for 20 independent observations, taken every 5 ms from the creation of the spin mixture up to 150 ms later. Each integrated cross section is then represented as a row on the space-time diagram in Fig. 1(c). The structures observed here are hallmarks of the nonlinear stage of MI, consisting of a gradual spatial transition between a harmonic outer edge and a central solitonic edge on either side of the barrier in the form of a DSW structure. In Fig. 1(c), dashed blue lines represent the speed of sound in this system, while red lines mark the speed of the MI envelope predicted by the 1D analytical expression Eq. (4) below. Good agreement between the expected MI growth rate and the experimental observations is found. The speed of sound in this system was determined experimentally to be $v_s = 2.0(1)$ μm/ms in a separate experiment, under similar conditions, where the barrier was suddenly doubled in strength to produce two outward traveling sound pulses, see, also, Supplemental Material (SM) [37]. In addition, we simulate the experimental conditions described above in both a 3D and an effective 1D model (detailed in SM [37], including Refs. [38,39]) shown in Figs. 1(d) and 1(e), respectively. In all cases, we observe excellent agreement with the experimental observations which are also in line with the analytical predictions of the MI growth. Intriguingly, these results also bear a striking resemblance to the experimental results of a single component with attractive interactions in a nonlinear optical fiber described by Kraych, *et al.* [13],

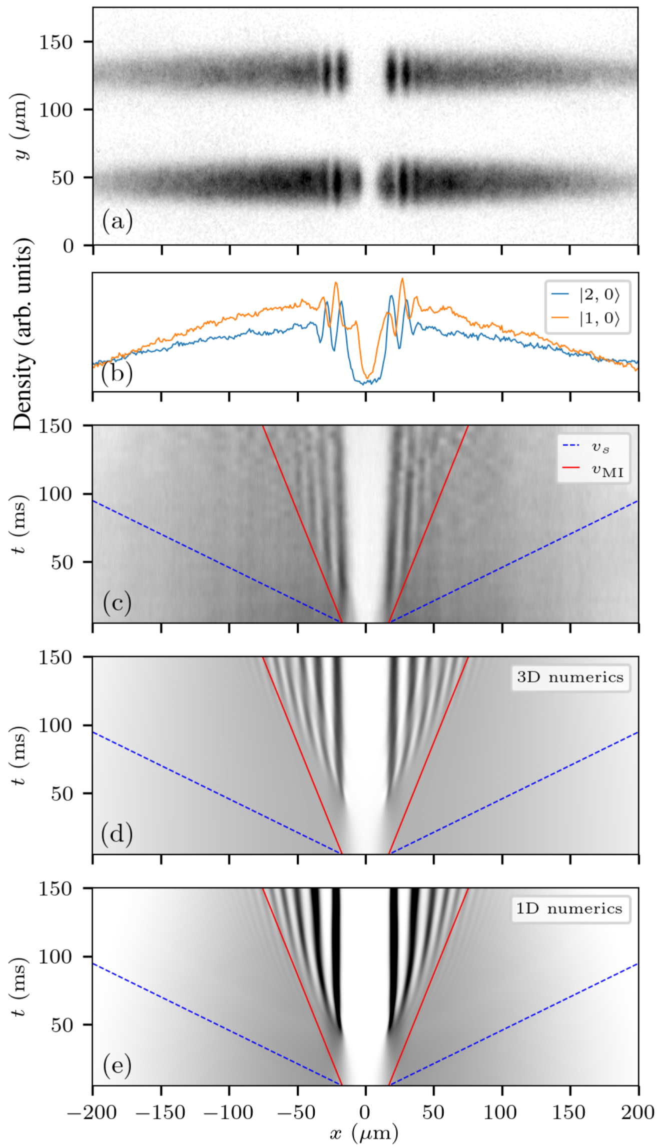

FIG. 1. Experimental and numerical demonstration of the nonlinear stage of MI from a repulsive barrier for an initially 50:50 mixture of $|2,0\rangle$ and $|1,0\rangle$ atoms. (a) Single-shot absorption image taken after 60 ms of evolution time showing the $|2,0\rangle$ state above the $|1,0\rangle$ state. (b) Integrated cross sections averaging over 20 independent experimental realizations corresponding to the absorption image in panel (a). (c) Spacetime evolution of the average integrated cross sections for the $|2,0\rangle$ state. The blue dashed lines show the experimentally determined speed of sound and the red lines depict the theoretically predicted MI expansion rate given in Eq. (4). Density evolution of the (d) integrated cross sections from 3D numerical simulations and (e) 1D simulations of the experimental conditions overlaid with the same lines as in panel (c).

even though we are working with a two-component system with purely repulsive interactions.

Modulationally unstable dynamics—For the numerical implementation of our setup, we begin with all atoms residing in the $|1,-1\rangle$ hyperfine state of ^{87}Rb. As a first step, the mean-field ground state of this single-component setup is obtained, via imaginary time propagation under the influence of the external potential of Eq. (2) containing a repulsive barrier. Next, we numerically simulate the experimental rf protocol by suddenly generating specific population mixtures, namely either a 50:50 or an 85:15 mixture of the $|1,0\rangle$ and $|2,0\rangle$ hyperfine states, respectively.

The ensuing dynamics of the two-component system is monitored through the coupled 3D Gross-Pitaevskii equations (GPEs) [4,40]

$$i\hbar\frac{\partial\Psi_F}{\partial t} = \left[-\frac{\hbar^2}{2M}\nabla^2_{\mathbf{r}} + V(\mathbf{r}) + \sum_{F'=1}^{2} g^{(3\mathrm{D})}_{FF'}|\Psi_{F'}|^2\right]\Psi_F, \tag{1}$$

where $\mathbf{r} = (x, y, z)$. The wave function of the $F = 1, 2$ hyperfine state is $\Psi_F \equiv \Psi_F(\mathbf{r}, t)$. Additionally, $g^{(3\mathrm{D})}_{FF'} = 4\pi N_{F'}\hbar^2 a_{FF'}/M$ are the intracomponent ($F = F'$) and intercomponent ($F \neq F'$) interaction coefficients related to the 3D s-wave scattering lengths $a_{FF'}$ (see below), M is the mass of ^{87}Rb atoms, while N_F refers to the F spin channel atom number. The external potential consists of the harmonic trap and the superimposed optically induced repulsive potential barrier

$$V(\mathbf{r}) = \frac{1}{2}M(\omega_x^2x^2 + \omega_y^2y^2 + \omega_z^2z^2) + V_0 e^{-2\left[\left(\frac{x}{s_x}\right)^2 + \left(\frac{y}{s_y}\right)^2\right]}. \tag{2}$$

The potential barrier is characterized by its height V_0 and widths (s_x, s_y), in line with the experimental values previously reported. This divides the BEC into two distinct, nonoverlapping density regions.

The relevant scattering lengths are $a_{11} = 100.86a_0$, $a_{22} = 94.57a_0$, and $a_{12} = a_{21} = 98.9a_0$, with a_0 denoting the Bohr radius. These scattering lengths result in an immiscible mixture. In the case of a large population imbalance among the hyperfine states, they lead to effectively attractive dynamics in the minority component, dictated by $a_{\rm eff} = a_{22} - a_{12}^2/a_{11} < 0$ [28,29,32]. This, in turn, allows us to observe focusing phenomena, such as the MI, in an otherwise repulsive environment. We emphasize that the use of the potential barrier is crucial for inducing the creation of experimentally repeatable and controllable counterpropagating DSWs. Indeed, without the barrier, an immiscible mixture would be subject to spontaneous MI [37]. Note, also, that the present protocol is in sharp contrast to the use of an attractive potential in Ref. [29], which facilitated rogue wave generation in a majority-minority scenario.

A typical example demonstrating the dynamical manifestation of MI and the resulting DSW formation is depicted in Fig. 1(d). Here, our 3D mean-field simulations are based on the experimental parameters of Fig. 1(c) and account for an atom-loss rate in the $|2,0\rangle$

state. The corresponding integrated density evolution, $n(x,t) = \int dydz|\Psi_F(x,y,z;t)|^2$, reveals the emission of two counter propagating DSWs featuring density undulations, both stemming from the Riemann-type initial condition emulated by the steep barrier. These DSWs, which describe the nonlinear stage of MI, expand with a speed represented by the red lines in Fig. 1(d). The relevant density modulations along with the characteristic speed of their envelope are more clearly discernible as compared to the experiment, see Figs. 1(c) and 1(d).

Nonlinear stage of MI—To obtain a theoretical handle on the observed phenomenology, we start with the following coupled 1D NLS system, written in dimensionless units:

$$iq_{j,t} + q_{j,xx} - 2(g_{j1}|q_1|^2 + g_{j2}|q_2|^2)q_j = 0. \tag{3}$$

Here, $j = 1, 2$, while constants g_{jk} (for $j, k = 1, 2$), quantify the effective 1D intracomponent ($j = k$) and intercomponent ($j \neq k$) interactions, and subscripts t and x denote temporal and spatial differentiation, respectively, of 1D wave function $q_j(x,t)$ of each component. It is known that, for an immiscible mixture (i.e., $g_{11}g_{22} < g_{12}^2$), MI can occur even in repulsive, $g_{jk} > 0$, BECs [41–43]. On the other hand, to the best of our knowledge, the MI-driven dynamical response has never been analytically characterized nor experimentally observed in such systems. It turns out that it is possible to prove (see SM [37] for the explicit derivation, including Ref. [44]) that, in such a scenario, the speed of the edge of the modulated region generalizes to $x(t) = \pm V_{2c}t$. The involved velocity reads

$$V_{2c} = 4\sqrt{-g_+ + \sqrt{g_-^2 + 4Q_1^2Q_2^2g_{12}^2}}, \tag{4}$$

with $g_\pm = g_{11}Q_1^2 \pm g_{22}Q_2^2$, and Q_j denoting the background amplitude of each component. The prediction of Eq. (4) can be compared to the analogous one of the single-component setting. The dynamics of the latter, characterized by the complex wave function $q(x,t)$, is governed by the NLS equation, $iq_t + q_{xx} - 2g|q|^2q = 0$, with $g < 0$ ($g > 0$) referring to the focusing (defocusing) nonlinearity. In this context, the edge of the modulated region propagates as $x(t) = \pm V_{\mathrm{NLS}}t$ [9,10], having velocity $V_{\mathrm{NLS}} = 4q_0\sqrt{-2g}$ (for background amplitude q_0).

For a highly particle-imbalanced two-component mixture, it is natural to take the limiting case of $Q_2 \ll Q_1$ in Eq. (4) in order to identify analogies with the single-component scenario (of the minority component). Expanding the inner square root and neglecting higher-order terms leads to

$$V_{2c} = 4Q_2\sqrt{-2g_{\mathrm{eff}}} + \mathcal{O}(Q_2^2). \tag{5}$$

Equation (5) is equivalent to V_{NLS} with an effective 1D coupling $g_{\mathrm{eff}} = g_{22} - g_{12}^2/g_{11}$ for the minority component of background amplitude Q_2. This is in line with the earlier analysis of the effective single-component (minority) reduction in [28,32]. However, we emphasize that Eq. (4) is valid in the more general case of arbitrary particle imbalanced BEC components.

The resultant density dynamics of one of the components of the 50:50 mixture stemming from the 1D GPE analysis is depicted in Fig. 1(e). Here, both the velocity of the MI edge, predicted by Eq. (4), and that of the experimentally determined speed of sound are depicted. Evidently, the observed density modulations exhibit a propagation speed that is in accordance with the analytical prediction for the 50:50 mixture. Additionally, the transition between particle balanced to highly imbalanced settings (and, hence, effectively single-component) is demonstrated in Fig. 2. Particularly, Figs. 2(a), 2(c), and 2(e) illustrate the spatiotemporal evolution of the wave function magnitude of the minority component, $|q_2(x,t)|$, accompanied by the edges of the MI in two-component (solid red line) and single-component (green dashed line) setups [see Eqs. (4) and (5), respectively]. Additionally, Figs. 2(b), 2(d), and 2(f) showcase specific snapshots at $t = 564$ ms. Here, for reference,

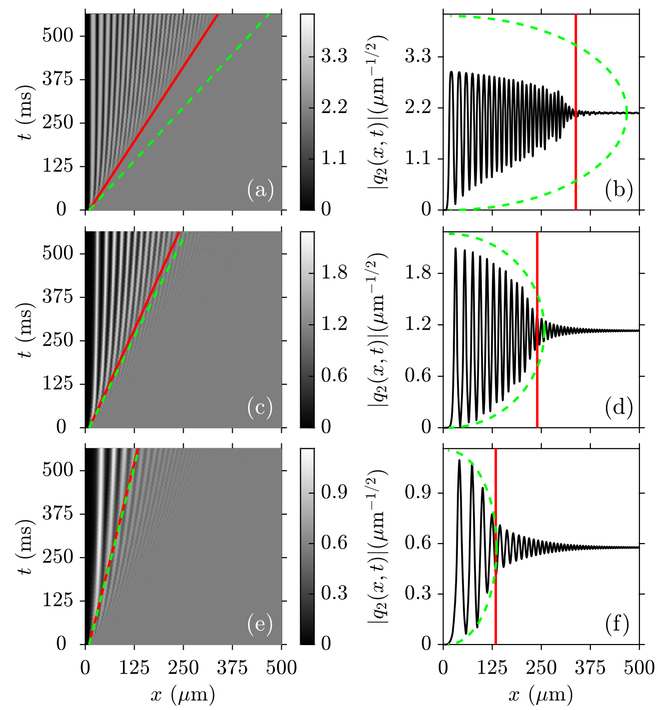

FIG. 2. Numerical 1D results of the nonlinear stage of MI of the $|2,0\rangle$ component in a (a) and (b) 50:50, (c) and (d) 85:15, and (e) and (f) 96:4 mixture. (a),(c),(e) Spatiotemporal evolution of the wave function magnitude of the minority component, $|q_2(x,t)|$. (b),(d),(f) Snapshot of $|q_2(x,t)|$ at $t = 564$ ms. Red lines mark the edge of the modulated region described by Eq. (4). Dashed green lines depict the envelope of the modulations dictated by Eq. (5). Because of symmetry, only the positive x axis is shown.

the envelope of the MI calculated from the single-component setting reported in Ref. [45] is also depicted (see more details in SM [37]). It can be readily seen that, as the particle imbalance increases, the MI occurs at longer evolution times, and the envelope of the resulting structure expands more slowly. Interestingly, the analytical estimates of the MI speed are in agreement with the outcome of the mean-field simulations. The MI speed and envelope profile approach their single-component counterpart with $g = g_{\rm eff}$ in the limit of $Q_2 \ll Q_1$, corroborating the relevant reduction.

Two-component dam-break problem—Finally, we extend our considerations to a geometry consisting of two barriers, each of which produces density modulations on either of its sides, as presented in Fig. 3. This more exotic scenario, resembling a matter-wave cavity (e.g., motivated by similar formulations in the case of solitonic collisions [46]), produces an interference pattern of the two DSWs emerging between the barriers as a result of the nonlinear stage of MI. An important byproduct of such interference in the semiclassical limit of focusing NLS models has been theoretically identified relatively recently in the work of Ref. [47]. There, it was found that this interference results in the formation of PS-like structures, a feature that was justified based on the analysis of the integrable properties of the relevant model. A realization of this recently proposed mechanism was reported in optics [48], but never in multiple components or in any form in quantum fluids, to the best of our knowledge. Here,

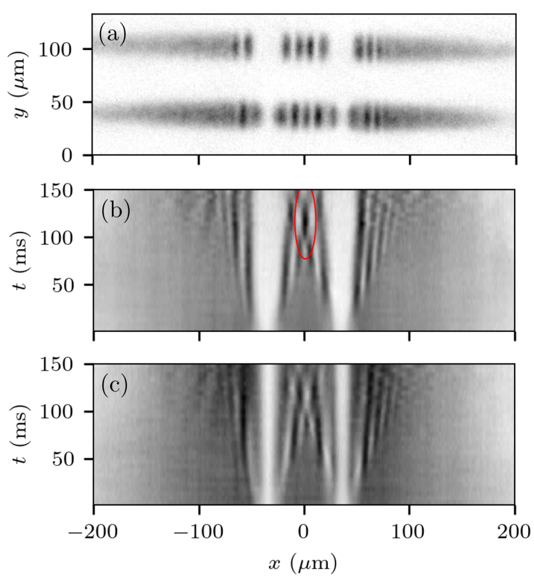

FIG. 3. Experimental images depicting DSW interaction produced by two barriers and subsequent PS formation in a 50:50 immiscible mixture. (a) Absorption image taken after 80 ms of evolution time with $|2,0\rangle$ appearing above $|1,0\rangle$. Spacetime evolution of the (b) $|2,0\rangle$ and (c) $|1,0\rangle$ components featuring complementary density profiles. A PS (red circle) appears at the center of the interference region.

we showcase the fact that even in our two-component, repulsive interaction generalization, both the numerical simulations [37], but also, crucially, the experimental data of Figs. 3(b) and 3(c) support the (unprecedented, to our knowledge) manifestation of this type of PS-generating dam-break interference in the realm of atomic BECs. Remarkably, this is true even for an equal mixture. In fact, we have further verified the existence of a PS-like structure by comparing its properties with those of the analytically available Peregrine waveform [34,49]. This reveals a very good agreement within the region of the PS-like core accompanied by a π phase jump between its core and tails, see, also, [37] for details. Also, we have checked experimentally that an increasing interbarrier distance leads to PS-like formation at longer times.

Conclusions—We have examined the nonlinear stage of MI in a two-component repulsive BEC of two hyperfine states of ^{87}Rb atoms, featuring a repulsive barrier. The manifestation of MI, which leads to DSW formation, is experimentally observed for immiscible species and theoretically analyzed for arbitrary ratios between the two components. Expanding on the analysis of the reducible majority-minority case, we favorably compare our experimental and numerical results with analytical formulas for the relevant wave function, its envelope, and propagation speed. Beyond the very good agreement between 3D numerics and experimental observations, and the definitive qualitative understanding enabled by the 1D analysis, we have also explored the more exotic scenario where two repulsive barriers, emulating a matter-wave cavity, induce the interference of multiple dam breaks. These, in line with relevant earlier theoretical predictions [47], have been verified to seed the emergence of a PS structure, providing an intriguing alternative avenue for its experimental realization compared to the gradient catastrophe one [50] recently realized within BECs [29].

This work provides exciting avenues for further exploration, including a quantitative characterization of the nonlinear stage of MI for arbitrary coefficients in multicomponent systems utilizing Whitham modulation theory [31,45], or the investigation of the impact of spinor settings or progressively higher dimensions, which may give rise to similar or other interesting patterns [3]. The identification of underlying correlation phenomena [19] emanating from the nonlinear stage of MI is of considerable interest. Another intriguing prospect is the study of possible universal features when the barrier is driven, triggering turbulent cascades [51,52].

Acknowledgments—A. R. R. acknowledges MCIN/AEI/10.13039/501100011033 from Grants No. PID2023-147112NB-C22; No. CNS2022-135529 through the “European Union NextGenerationEU/PRTR”; No. CEX2024-001451-M through the “Unit of Excellence María de Maeztu 2025–2031” Award to the

Institute of Cosmos Sciences; and by the Generalitat de Catalunya, Grant No. 2021SGR01095. P. E. acknowledges funding from NSF through Grant No. PHY-2207588 as well as support from a Boeing Endowed Professorship at WSU. This research was also supported in part by the National Science Foundation under Grant No. NSF PHY-1748958. S. I. M. acknowledges support from the Missouri Science and Technology, Department of Physics, Startup Fund. This material is also based upon work supported by the US National Science Foundation under Grants No. PHY-2110030, No. PHY-2408988, and No. DMS-2204702 (P. G. K.).

Data availability—The data that support the findings of this Letter are not publicly available upon publication because it is not technically feasible and/or the cost of preparing, depositing, and hosting the data would be prohibitive within the terms of this research project. The data are available from the authors upon reasonable request.

[1] V. Zakharov and L. Ostrovsky, Physica (Amsterdam) **238D**, 540 (2009).
[2] P. J. Everitt, M. A. Sooriyabandara, M. Guasoni, P. B. Wigley, C. H. Wei, G. D. McDonald, K. S. Hardman, P. Manju, J. D. Close, C. C. N. Kuhn, S. S. Szigeti, Y. S. Kivshar, and N. P. Robins, Phys. Rev. A **96**, 041601 (2017).
[3] C.-A. Chen and C.-L. Hung, Phys. Rev. Lett. **125**, 250401 (2020).
[4] P. G. Kevrekidis, D. J. Frantzeskakis, and R. Carretero-González, *The Defocusing Nonlinear Schrödinger Equation: From Dark Soliton to Vortices and Vortex Rings*, Other Titles in Applied Mathematics (Society for Industrial and Applied Mathematics, Philadelphia, 2015).
[5] Y. S. Kivshar and G. P. Agrawal, *Optical Solitons: From Fibers to Photonic Crystals* (Academic Press, New York, 2003), pp. 1–540.
[6] M. Ablowitz, *Nonlinear Dispersive Waves, Asymptotic Analysis and Solitons* (Cambridge University Press, Cambridge, England, 2011).
[7] M. Kono and M. Skorić, *Nonlinear Physics of Plasmas* (Springer-Verlag, Heidelberg, 2010).
[8] V. E. Zakharov and A. A. Gelash, Phys. Rev. Lett. **111**, 054101 (2013).
[9] G. Biondini and D. Mantzavinos, Phys. Rev. Lett. **116**, 043902 (2016).
[10] G. El', A. Gurevich, V. Khodorovskiĭ, and A. Krylov, Phys. Lett. A **177**, 357 (1993).
[11] G. B. Whitham, Proc. R. Soc. A **283**, 238 (1965).
[12] G. Biondini and G. Kovačič, J. Math. Phys. (N.Y.) **55**, 031506 (2014).
[13] A. E. Kraych, P. Suret, G. El, and S. Randoux, Phys. Rev. Lett. **122**, 054101 (2019).
[14] F. Copie, S. Randoux, and P. Suret, Rev. Phys. **5**, 100037 (2020).
[15] F. Bonnefoy, A. Tikan, F. Copie, P. Suret, G. Ducrozet, G. Prabhudesai, G. Michel, A. Cazaubiel, E. Falcon, G. El, and S. Randoux, Phys. Rev. Fluids **5**, 034802 (2020).
[16] G. Biondini, S. Li, D. Mantzavinos, and S. Trillo, SIAM Rev. **60**, 888 (2018).
[17] I. Bloch, J. Dalibard, and W. Zwerger, Rev. Mod. Phys. **80**, 885 (2008).
[18] C. Gross and I. Bloch, Science **357**, 995 (2017).
[19] S. I. Mistakidis, A. G. Volosniev, R. E. Barfknecht, T. Fogarty, T. Busch, A. Foerster, P. Schmelcher, and N. T. Zinner, Phys. Rep. **1042**, 1 (2023).
[20] K. E. Strecker, G. B. Partridge, A. G. Truscott, and R. G. Hulet, Nature (London) **417**, 150 (2002).
[21] K. E. Strecker, G. B. Partridge, A. G. Truscott, and R. G. Hulet, New J. Phys. **5**, 73 (2003).
[22] J. H. V. Nguyen, D. Luo, and R. G. Hulet, Science **356**, 422 (2017).
[23] P. J. Everitt, M. A. Sooriyabandara, M. Guasoni, P. B. Wigley, C. H. Wei, G. D. McDonald, K. S. Hardman, P. Manju, J. D. Close, C. C. N. Kuhn, S. S. Szigeti, Y. S. Kivshar, and N. P. Robins, Phys. Rev. A **96**, 041601(E) (2017).
[24] C.-A. Chen and C.-L. Hung, Phys. Rev. Lett. **125**, 250401 (2020).
[25] C.-A. Chen and C.-L. Hung, Phys. Rev. Lett. **127**, 023604 (2021).
[26] S. Banerjee, K. Zhou, S. K. Tiwari, H. Tamura, R. Li, P. Kevrekidis, S. I. Mistakidis, V. Walther, and C.-L. Hung, Phys. Rev. Lett. **135**, 073401 (2025).
[27] Y. V. Kartashov, B. A. Malomed, and L. Torner, Rev. Mod. Phys. **83**, 247 (2011).
[28] B. Bakkali-Hassani, C. Maury, Y.-Q. Zou, É. Le Cerf, R. Saint-Jalm, P. C. M. Castilho, S. Nascimbene, J. Dalibard, and J. Beugnon, Phys. Rev. Lett. **127**, 023603 (2021).
[29] A. Romero-Ros, G. C. Katsimiga, S. I. Mistakidis, S. Mossman, G. Biondini, P. Schmelcher, P. Engels, and P. G. Kevrekidis, Phys. Rev. Lett. **132**, 033402 (2024).
[30] G. B. Whitham, *Linear and Nonlinear Waves* (John Wiley & Sons, New York, 2011).
[31] G. El and M. Hoefer, Physica (Amsterdam) **333D**, 11 (2016).
[32] Z. Dutton and C. W. Clark, Phys. Rev. A **71**, 063618 (2005).
[33] B. Bakkali-Hassani, C. Maury, S. Stringari, S. Nascimbene, J. Dalibard, and J. Beugnon, New J. Phys. **25**, 013007 (2023).
[34] A. Romero-Ros, G. C. Katsimiga, S. I. Mistakidis, B. Prinari, G. Biondini, P. Schmelcher, and P. G. Kevrekidis, Phys. Rev. A **105**, 053306 (2022).
[35] M. A. Hoefer, M. J. Ablowitz, I. Coddington, E. A. Cornell, P. Engels, and V. Schweikhard, Phys. Rev. A **74**, 023623 (2006).
[36] M. E. Mossman, M. A. Hoefer, K. Julien, P. G. Kevrekidis, and P. Engels, Nat. Commun. **9**, 4665 (2018).
[37] See Supplemental Material at http://link.aps.org/supplemental/10.1103/6jsr-f8q1 for additional details and complementary results.
[38] L. Salasnich, A. Parola, and L. Reatto, Phys. Rev. A **65**, 043614 (2002).
[39] A. I. Nicolin and M. C. Raportaru, Physica (Amsterdam) **389A**, 4663 (2010).

[40] L. P. Pitaevskii and S. Stringari, *Bose-Einstein Condensation*, Oxford Science Publications No. 116 (Clarendon Press, Oxford, 2003).
[41] P. Tommasini, E. J. V. de Passos, A. F. R. de Toledo Piza, M. S. Hussein, and E. Timmermans, Phys. Rev. A **67**, 023606 (2003).
[42] K. Kasamatsu and M. Tsubota, Phys. Rev. A **74**, 013617 (2006).
[43] K. Kasamatsu and M. Tsubota, Phys. Rev. Lett. **93**, 100402 (2004).
[44] F. W. Olver, D. W. Lozier, D. W. Boisvert, and C. W. Clark, *NIST Handbook of Mathematical Functions* (Cambridge University Press, Cambridge, England, 2010), ISBN 9780521140638.
[45] G. Biondini, Phys. Rev. E **98**, 052220 (2018).
[46] S. Lannig, C.-M. Schmied, M. Prüfer, P. Kunkel, R. Strohmaier, H. Strobel, T. Gasenzer, P. G. Kevrekidis, and M. K. Oberthaler, Phys. Rev. Lett. **125**, 170401 (2020).
[47] G. A. El, E. G. Khamis, and A. Tovbis, Nonlinearity **29**, 2798 (2016).
[48] F. Audo, B. Kibler, J. Fatome, and C. Finot, Opt. Lett. **43**, 2864 (2018).
[49] D. H. Peregrine, ANZIAM J. **25**, 16 (1983).
[50] M. Bertola and A. Tovbis, Commun. Pure Appl. Math. **66**, 678 (2013).
[51] N. Navon, A. L. Gaunt, R. P. Smith, and Z. Hadzibabic, Nature (London) **539**, 72 (2016).
[52] N. Navon, R. P. Smith, and Z. Hadzibabic, Nat. Phys. **17**, 1334 (2021).